Dynamics of shear-induced ATP release from red blood cells

Jiandi Wan, William D. Ristenpart*, and Howard A. Stone†

School of Engineering and Applied Sciences, Harvard University, 29 Oxford Street, Cambridge, MA 02138

Edited by Sheldon Weinbaum, The City College of the City University of New York, New York, NY, and approved September 2, 2008 (received for review June 15, 2008)

Adenosine triphosphate (ATP) is a regulatory molecule for many cell functions, both for intracellular and, perhaps less well known, extracellular functions. An important example of the latter involves red blood cells (RBCs), which help regulate blood pressure by releasing ATP as a vasodilatory signaling molecule in response to the increased shear stress inside arterial constrictions. Although shear-induced ATP release has been observed widely and is believed to be triggered by deformation of the cell membrane, the underlying mechanosensing mechanism inside RBCs is still controversial. Here, we use an *in vitro* microfluidic approach to investigate the dynamics of shear-induced ATP release from human RBCs with millisecond resolution. We demonstrate that there is a sizable delay time between the onset of increased shear stress and the release of ATP. This response time decreases with shear stress, but surprisingly does not depend significantly on membrane rigidity. Furthermore, we show that even though the RBCs deform significantly in short constrictions (duration of increased stress <3 ms), no measurable ATP is released. This critical timescale is commensurate with a characteristic membrane relaxation time determined from observations of the cell deformation by using high-speed video. Taken together our results suggest a model wherein the retraction of the spectrin-actin cytoskeleton network triggers the mechanosensitive ATP release and a shear-dependent membrane viscosity controls the rate of release.

mechanotransduction | microfluidic | RBCs

As the central component of the human circulatory system, RBCs have evolved highly specific mechanisms for responding to variations in the local environment. One key but poorly understood response mechanism involves the release of ATP to the extracellular space, which occurs in response to small changes in pH (1), oxygen concentration (2) or osmotic pressure (3). Although ATP is well known as the energy source for intracellular functions, extracellular ATP plays an important role as a signaling molecule in a variety of physiological processes. For example, the ATP released from RBCs helps regulate vascular tone by binding with purigenic receptors on endothelial cells, which then respond by releasing nitric oxide, a potent vasodilator, into the surrounding smooth muscle cells (1, 4–6). In addition, a variety of diseases are linked to impaired ATP release from RBCs, including cystic fibrosis (7), pulmonary hypertension (8), and diabetes (9, 10). Furthermore, extracellular ATP is known to inhibit growth of breast and lung tumors (11, 12) and plays a role in the inflammation response to wounds (13). Knowledge of the circumstances under which RBCs release ATP is crucial for designing effective therapeutic strategies.

A fundamental characteristic of RBCs is that they regularly encounter variations in hydrodynamic shear stress, especially on entering or exiting arterioles and capillaries (14). A mounting body of evidence suggests that RBCs respond to these variations in shear stress by releasing ATP (4, 15–19). Sprague *et al.* (4) proposed that the increased shear stress inside narrower channels causes the RBCs to deform, and that the deformation triggers release of ATP. They corroborated their hypothesis by sending RBCs through filter paper with different mean pore sizes; for smaller pore sizes (i.e., higher shear stresses), more ATP was released (4). Further investigations focused on more controlled shear-stress conditions by using microbore tubing (15, 16) and microfluidic channels (17–19), confirming that the amount of ATP released depended on the magnitude of shear stress (i.e., tubing diameter or fluid velocity) and the duration of the shear stress (i.e., length of the tubing). Addition of chemicals that rigidify RBC membranes (e.g., diamide) decreased the amount of ATP released, which suggested that deformation of the cell was a necessary trigger (19).

Many questions remain, however, about the *dynamics* of deformation-induced ATP release. For example, how much deformation yields how much ATP? How quickly do the RBCs release ATP in response to an increase in shear stress? Are RBCs sensitive to the absolute magnitude of the shear stress, or the rate of change in shear stress, or both? Which aspects of the deformations are most significant in triggering release? Because the mechanism of mechanosensitive ATP release from RBCs is controversial and several hypotheses have been proposed (20–22), information about the dynamics of ATP release will be helpful for illuminating the mechanotransduction pathways and the underlying biochemical release mechanisms. Furthermore, these studies may help reveal how to compensate for impaired ATP release in various disease states.

In this work, we use a microfluidic approach to measure the dynamics of shear-induced ATP release from RBCs. Our *in vitro* experimental measurements involve a series of microfluidic channels that include a narrow constriction. The higher shear stress in the constriction serves as the mechanical stimulus on the cells, the magnitude and duration of which are varied in different devices by changing, respectively, the width and length of the constriction. Because position and time are interchangeable in steady-state microfluidic systems, we are able to measure the dynamics of ATP release with millisecond resolution.

We measured the amount of released ATP by counting the photons emitted from the standard luciferase-ATP bioluminescent reaction, and in a separate set of experiments we directly visualized the extent of the deformation of individual cells by using high-speed video. We identify four main points: (*i*) a significant time delay transpires between the onset of increased shear stress and the release of ATP; (*ii*) increasing the effective rigidity of the RBCs decreases the amount of ATP released, but has a negligible effect on the delay time; (*iii*) no measurable ATP is released in channels of sufficiently small length despite large

Author contributions: J.W., W.D.R., and H.A.S. designed research; J.W. performed research; J.W., W.D.R., and H.A.S. analyzed data; and J.W., W.D.R., and H.A.S. wrote the paper.

The authors declare no conflict of interest.

This article is a PNAS Direct Submission.

*Present address: Department of Chemical Engineering and Materials Science and Department of Food Science and Technology, University of California, 1 Shields Avenue, Davis, CA 95616.

†To whom correspondence should be addressed. E-mail: has@seas.harvard.edu.

This article contains supporting information online at www.pnas.org/cgi/content/full/0805779105/DCSupplemental.

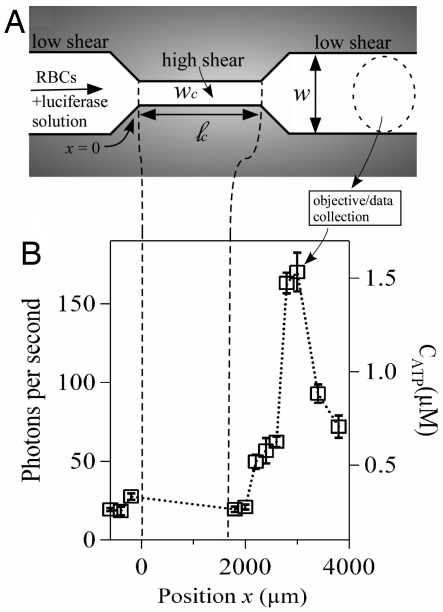

Fig. 1. Microfluidic approach for shear-triggered release of ATP. (*A*) Schematic of the experimental apparatus (not to scale). A mixture of RBCs and luciferase/luciferin solution are pumped through a microfluidic constriction. (*B*) Representative experimental measurements of the photon emission rate resulting from the reaction between luciferase/luciferin and ATP, measured versus position along the channel ($\ell_c = 1{,}600\ \mu$m and $w_c = 20\ \mu$m). The position $x = 0$ is defined as where the entrance to the constriction is located. The approximate ATP concentration (C_{ATP}) converted from the calibration curve (Fig. S1) is shown on the right axis. We focus here only on light collected outside of the constriction; no appreciable signal was measured inside the constriction (Fig. S2). The error bars are reported as the standard error of the mean ($n = 5$ different measurements). Note that the photon emission rate increases far downstream from the constriction.

deformation of the RBCs; and (*iv*) the critical duration of increased shear stress needed to activate the release process is commensurate with a membrane relaxation time. These results suggest that the ATP release is mechanically coupled to the *retraction* of the cell membrane network, not just the initial deformation.

Microfluidic Design. A representative microfluidic channel used in our experiments is sketched in Fig. 1*A*. The "wide" sections of the microchannel, before and after the constriction, have a uniform width $w = 100\ \mu$m, whereas the constriction itself has a width $w_c < 100\ \mu$m. Because the height h of the microchannel is uniform ($h = 38\ \mu$m), the magnitude of the average shear rate and the corresponding shear stress in the constriction depend on w_c; smaller values of w_c provide a larger average shear stress. By varying the length ℓ_c of the constriction in different devices, the amount of time the RBCs experience the higher shear stress (i.e., the duration) can be varied systematically.

To begin an experiment, a hematocrit of 10% by volume ($\approx 5 \times 10^8$ cells per milliliter) of RBCs in solution with luciferase/luciferin was pumped into the microchannel at a constant volumetric flow rate, $Q = 3\ \mu$l/min. This flow rate yields an average flow speed $u \approx 1.3$ cm/s upstream of the constriction, which corresponds to a Reynolds number of ≈ 1 (here, the Reynolds number $\mathrm{Re} = \rho u h/\mu$, where for 10% hematocrit $\rho \approx 10^3$ kg·m^{-3} and $\mu \approx 10^{-3}$ kg·m^{-1}·s^{-1}). The ATP released from the RBCs reacted with the luciferase/luciferin to produce photons, which were counted by using a photon-counting photomultiplier setup attached to a microscope. Approximate ATP concentrations were then obtained based on an independently measured calibration curve [supporting information (SI) Fig. S1]. We note that the typical shear rates in the constriction are comparable to those found in arterioles tens of micrometers in diameter (23).

By translating the microscope objective to different positions (x) along the channel, the amount of ATP released was measured versus distance from the beginning of the constriction ($x = 0$; cf. Fig. 1*A*.). For time-invariant flows in microfluidic channels, the spatial position and elapsed time are interchangeable. We use this space–time equivalence to obtain the time of release of ATP after the abrupt velocity change in the constriction. For our flow velocities and microscope magnification, the ATP release was detected temporally with a resolution of a few milliseconds. We focus here only on light collected outside of the constriction; no appreciable signal was measured inside the constriction (Fig. S2). The RBCs are small compared with the channel size, so each cell experienced a different shear stress depending on its specific position in the channel. Consequently, the measured number of photons represents the collective influence of many different cells releasing ATP, and the measurements reflect the average effect of the increased average shear stress in the constriction. By using high-speed video (see below), we did not observe any cell lysis under the range of applied shear stresses used in this work. Thus, increases in light emission compared with the background level upstream of the constriction are a consequence of the cellular response to the increased shear inside the constriction.

Results

Shear-Induced ATP Release. Data from a typical experimental trial in a constriction with $w_c = 20\ \mu$m and $\ell_c = 1{,}600\ \mu$m are presented in Fig. 1*B*. The average speed in the constriction was ≈ 6.6 cm/s, so the cells traversed the constriction in ≈ 24 ms. Upstream of the constriction, a baseline level of ≈ 20 photons per second varied little with position (Fig. S3). Inside the constriction, a lower but spatially invariant photon emission rate was observed, presumably because of the smaller signal collection area (Fig. S2). After the constriction, the photon emission rate remained unchanged until approximately $x \approx 2{,}000\ \mu$m, where it increased rapidly to a maximum of ≈ 175 photons per second near $x \approx 3{,}000\ \mu$m. At larger distances, the photon emission rate decreased, eventually reaching the baseline rate sufficiently far downstream.

The most striking feature in Fig. 1*B* is that most of the light is emitted far downstream of the constriction. Care must be taken to interpret this result properly, however. First, we convert the spatial positions to elapsed times based on the time-invariant flow rate Q in the channel. The total time (τ) that transpires from the constriction entrance at $x = 0$ to arbitrary x is estimated by using the average flow speeds inside (u_c) and outside (u_{out}) of the constriction, that is,

$$\tau = \tau_c + \tau_{\mathrm{out}} = \frac{\ell_c}{u_c} + \frac{x - \ell_c}{u_{\mathrm{out}}} = \frac{h}{Q}\left[w_c \ell_c + w(x - \ell_c)\right] \qquad [1]$$

where the flow rate $Q = u_c h w_c = uhw$. Substitution of the appropriate values for this experiment shows that the position where photon emission began to increase ($x \approx 2{,}000\ \mu$m) corresponds to a total elapsed time of $\tau \approx 54$ ms.

This result suggests that there is a considerable lag time between the onset of increased shear stress and the release of ATP. To interpret this result, we recognize that the observed delay depends on three different physical processes: (*i*) the mechanotransduction time required for a cell to respond to the onset of increased shear stress; (*ii*) the diffusion time required for released ATP to find the luciferase–luciferin complex; and (*iii*) the biochemical reaction time once the ATP binds to the complex. Accordingly, estimates of the influence of diffusion and reaction allow us to extract a timescale for mechanotrans-

duction. Based on the micromolar enzyme concentrations used in our experiments, the typical diffusion time for released ATP to find the enzyme complex is less than a millisecond, which indicates that the influence of diffusion on the observed delay time is negligible.

To gauge the impact of kinetics, we repeated our experiment by using a 20-fold increase in enzyme concentration, and we observed a similar delay time and peak magnitude (Fig. S2). This result indicates that the measured lag time is not simply due to chemical kinetics limited by the enzyme concentration. Moreover, as discussed in the next section, we find that the overall delay time is a function of the magnitude of shear stress in the constriction, which is inconsistent with a delay based entirely on chemical kinetics. In their seminal work on firefly luciferase, DeLuca and McElroy (24, 25) established that the biochemical reaction between the luciferase–luciferin complex and ATP has a 25-ms delay time before light is emitted. They attributed this delay to a slow conformational change of the ATP–luciferin–luciferase complex, and they found that the delay time was independent of the ATP and enzyme concentrations. The key point is that the reaction delay time is less than the total delay time observed in our experiments. Given that the diffusion timescale is negligible, the difference between our observed delay time and the 25-ms luciferase reaction time provides an estimate for the timescale of the cellular mechanotransduction events. For the measured delay time of 54 ms, we conclude that the RBCs began releasing significant amounts of ATP ≈29 ms after the onset of increased shear stress.

Experiments with the same average shear stress but different durations show that this mechanotransduction timescale is robust. Results for six different devices with varied ℓ_c (ranging from 100 to 3,200 μm) but the same constriction width ($w_c = 20$ μm) are presented in Fig. 2*A*, in which the x coordinates have been converted to elapsed time by means of Eq. **1**. For $\ell_c \geq 400$ μm, the results are qualitatively similar to Fig. 1*B*, that is, a significant delay occurred before the light signal increased. The approximate time at which the light signal began to increase (the delay time), indicated by the gray arrows in Fig. 2*A*, is plotted versus the duration τ_c of the increased shear stress in Fig. 2*B*. The gray arrows are placed only on data points where the subsequent data point is at least 30% larger and continues to trend upward. For $\tau_c \geq 3$ ms, the average total delay time is 55 ms with a standard deviation of ±10 ms. Subtraction of the ATP-luciferase reaction time yields an estimated mechanotransduction time of 30 ± 10 ms.

The data in Fig. 2 indicate two other key features about the cellular response. First, for sufficiently short constrictions little or no additional ATP is released. Specifically, no noticeable increase in light emission was observed for $\ell_c = 100$ μm and only a small increase for $\ell_c = 200$ μm, but a significant increase was observed for $\ell_c = 400$ μm. Given the detection limits of our experimental apparatus, the released ATP in the 100 μm and 200 μm channels (if any) was <100 nM (cf. Fig. S1*B*). By Eq. 1, the critical channel length of 200–400 μm indicates that there is a threshold duration of applied shear stress of approximately $\tau_c \approx 3$–6 ms required to trigger release of a significant amount of ATP. We identify this critical duration as a mechanotransduction *activation* time. We note that the cells tend to concentrate toward the center of the channel (26) as a consequence of the hydrodynamic lift experienced by the deformable cells. Because the flow is approximately parabolic, some fraction of the cells may traverse the constriction at most about twice as fast as the average liquid speed. The duration of applied higher shear stress experienced by these RBCs will be reduced, but this leads to at most a factor of two decrease in the activation time.

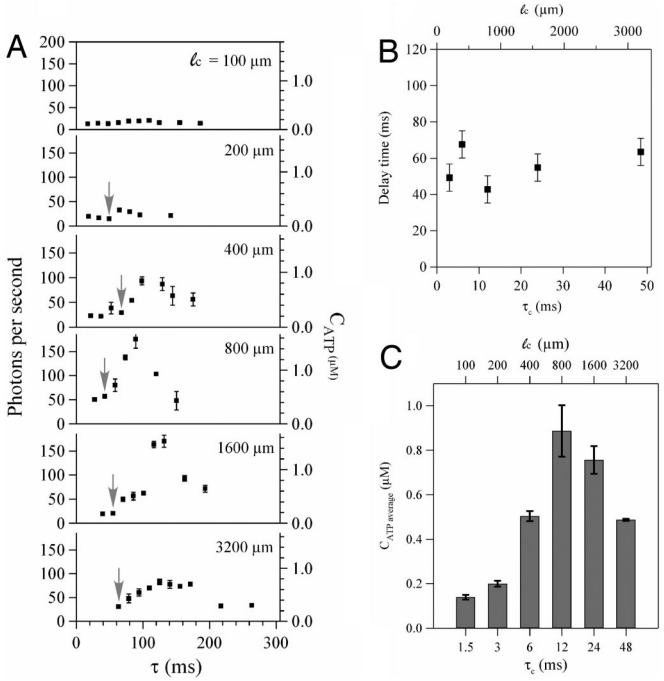

Fig. 2. Effect of the constriction length (i.e., the duration of increased shear stress) on ATP release in constrictions with fixed width ($w_c = 20$ μm). (*A*) The photon emission rate versus elapsed time (measured from the constriction entrance) for six different channels with different lengths ($\ell_c = 100$–3,200 μm). Arrows indicate the approximate time at which the photon rate begins to increase. The error bars are reported as the standard error of the mean ($n = 5$). (*B*) The delay time observed from *A* versus the duration of the increased shear stress (τ_c) for five different channels with fixed widths ($w_c = 20$ μm) but different lengths ($\ell_c = 200$–3,200 μm). The error bars are reported as uncertainty bars between data points. (*C*) The average released ATP concentration versus the duration of the increased shear stress (τ_c). The error bars are reported as the standard error of the mean ($n = 5$). All reported times are estimates based on the average flow rate, *cf.* Eq. 1.

A second key feature revealed in Fig. 2 is that, for a given shear stress, the average amount of released ATP reaches a maximum value as ℓ_c increases. Here, we define the average ATP concentration as $(1/L)\int_0^L C_{ATP}dx$, where L encompasses the distance over which measurements were performed. Averages were estimated from the data in Fig. 2*A* via trapezoidal quadrature and plotted in Fig. 2*C* versus the duration of the applied shear stress. Below the activation time of 3–6 ms there is little or no additional ATP released compared with the baseline, but there is a maximum at $\ell_c = 800$ μm. These data can be interpreted in terms of the available intracellular ATP concentration, which for RBCs is ≈10 mM (5, 27, 28). Only 1% or less of the intracellular ATP molecules is believed to be released for signaling purposes (5). For our experiments with 10% hematocrit (the number density of cells inside the channel was confirmed by image analysis of representative samples), the average concentration in a representative volume is 1 mM, so 1% of this value is 10 μM. In Fig. 2*C*, the average amount of released ATP increases up to ≈1 μM. This calculation suggests that the cells release only a fraction of their intracellular ATP in response to the higher shear stress in the constriction.

Effect of Deformation. Although the extent of mechanical deformation of the RBC membrane has been hypothesized to control shear-induced ATP release (7, 18), direct observations of the deformation of individual cells and their corresponding ATP release have not been reported. To elucidate the influence of deformation, we performed two separate experiments

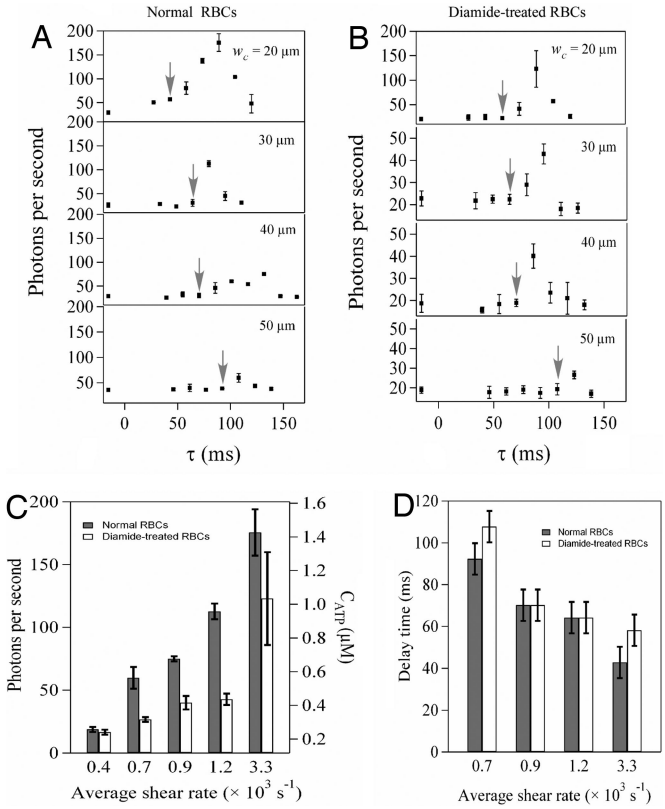

Fig. 3. Effect of the constriction width (i.e., the magnitude of increased shear rate) on ATP release in constrictions with fixed length (ℓ_c = 800 μm). The photon emission rate from normal (*A*) and diamide-treated (*B*) blood cells versus elapsed time (measured from the constriction entrance) for four different channels with different widths (w_c = 20–50 μm). Note the different scales for photon emission rate in *A* and *B*. Arrows indicate the approximate time at which the photon emission rate begins to increase. The error bars are reported as the standard error of the mean (n = 3). (*C*) The maximum photon emission rate for normal (filled bars) and diamide-treated (open bars) blood cells versus the average shear rate. The error bars are reported as the standard error of the mean (n = 3). (*D*) The delay time for normal (filled bars) and diamide-treated (open bars) RBCs versus the average shear rate in the constriction for the four different channels. The error bars are reported as uncertainty bars between data points.

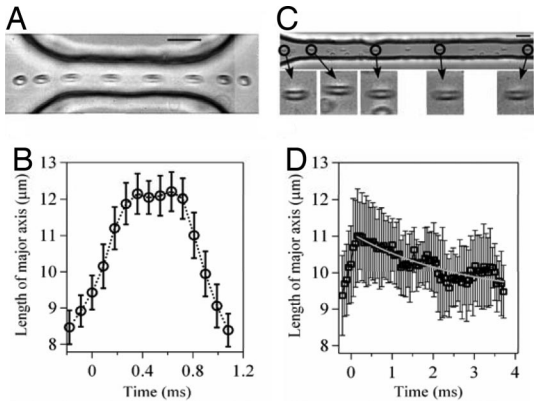

Fig. 4. Visual observations of the deformations of RBCs recorded with high-speed video at 11,000 frames per second. (*A*) Superimposed series of time-lapse images showing the deformation of an individual RBC passing through a short constriction (ℓ_c = 100 μm and w_c = 20 μm). (Scale bar, 20 μm.) Flow direction is left to right. (*B*) Average RBC length (measured in the flow direction) versus time for cells passing through the short constriction shown in *A*. Data averaged from 20 cells. (*C*) Superimposed series of time-lapse images showing the deformation of an RBC passing through a long constriction (ℓ_c = 800 μm and w_c = 20 μm). Only the initial part of the constriction channel is shown. The magnified images show an individual cell at different positions in the constriction channel. (Scale bar, 20 μm.) (*D*) Average RBC length versus time for cells passing through the long constriction shown in *C*. Data averaged from 22 cells. The gray line is a single exponential fit with characteristic relaxation time 2.7 ms. The error bars in *D* are larger than in *B* because of the lower magnification.

aimed at correlating the ATP release with visual measurements of deformation.

First, we examined the effect of the shear stress magnitude on the *dynamics* of ATP release for both normal and diamide-treated RBCs. Diamide is an oxidant that rigidifies RBCs by cross-linking sulfide groups in the spectrin network attached to the cell membrane (29, 30). Four independent experiments were conducted by using devices with the same constriction length (ℓ_c = 800 μm) but different widths (w_c = 20, 30, 40, 50 μm). Fig. 3 *A* and *B* shows the photon emission rate as a function of the elapsed time (τ) for normal and diamide-treated RBCs, respectively, for each of the four constriction widths. The plots are qualitatively similar to those shown in Fig. 2, but here we see that not only the magnitude of the released ATP, but also the approximate delay time (indicated by gray arrows) depend on the applied shear stress. Estimating the average shear rate as $\gamma \approx u_c/h \approx Q/w_c h^2$, Fig. 3*C* show that for wider constrictions (lower average shear stresses) the amount of ATP released decreases until it reaches the baseline value at $w_c = w$ (i.e., no constriction). The amount of released ATP scales approximately linearly with the average shear rate (Fig. S4).

Cells treated with diamide exhibited the same trend as normal cells, but invariably released less ATP. More interestingly, the delay times decrease with shear rate for both normal and diamide-treated RBCs, as shown in Fig. 3*D*. Depending on the shear stress, the total delay time varied between ≈50 and 100 ms, so subtraction of the chemical reaction timescale (25 ms) indicates that the cellular response time varies between 25 and 75 ms. Surprisingly, the delay times for the normal and diamide-treated RBCs at any given shear rate are comparable. Our results are consistent with previous observations (18) that the diamide treatment decreases the magnitude of the ATP release, but we find that the cellular response time is insensitive to the presence of diamide.

Treatment with diamide is an indirect test of the relationship between the membrane deformability and the amount of released ATP, so we performed a second set of experiments to examine the deformation directly by using high-speed video. We focus here on two constrictions with the same width (w_c = 20 μm) but different lengths (ℓ_c = 100 μm and 800 μm) to illustrate the key differences in the cellular response between a system that releases significant amounts of ATP versus one that does not (cf. Fig. 2*A*). In the shorter geometry (Fig. 4*A*), the cell undergoes a stretching deformation as it enters the constriction channel and compresses on exiting. The average length of the cell, measured in the streamwise direction and averaged over >20 different cells, is plotted versus time in Fig. 4*B*. The cells are stretched by ≈40% on entering the constriction, but rapidly recover to their original shape on exiting the constriction. Although these data show that considerable deformation occurs, recall from Fig. 2*A* that no observable ATP is released for constrictions this short (ℓ_c = 100 μm). We conclude that a large deformation of the cell is, by itself, insufficient to trigger release of a significant amount of ATP.

In contrast, significant amounts of ATP are released with longer constrictions, but the magnitude of deformation in the longer channel (Fig. 4*C*, ℓ_c = 800 μm) is approximately the same as in the shorter channel (Fig. 4*A*). The key difference, however,

is that significant relaxation of the cell occurs inside the constriction. Measurements of the average streamwise length of the cell inside the constriction (Fig. 4*D*) show that the cells slowly relax back to their original shape with a timescale of ≈3 ms. In comparison, on exiting the shorter constriction, the cells return to their original shape in only 0.4 ms (Fig. 4*B*).

Discussion

Our results indicate that there are two distinct timescales associated with mechanotransductive release of ATP from RBCs. The first timescale is the activation time, which we estimate to be 3–6 ms based on the minimum constriction length necessary to induce significant ATP release. Deformations that occur on shorter timescales do not induce ATP release. The second timescale, after activation, is associated with the time required for the release of ATP in response to the onset of increased shear stress. This timescale varies from 25 to 75 ms depending on the magnitude of the increased shear stress, but is insensitive to the membrane rigidity. This timescale is consistent with a *local* physiological influence of ATP release after increased shear stress in the microcirculation; for example, based on a 30-ms delay time, single cells moving in narrow constrictions at a speed of 0.2 cm/s would release ATP as an extracellular signaling molecules after only translating 60 μm, which is <10–12 cell lengths.

The direct visual observations of cellular deformations (cf. Fig. 4) suggest that the RBCs "sense" the length of the constriction according to the time required for the cell membrane to evolve to a new steady shape in the channel. One possible mechanotransductive mechanism involves the spectrin-actin network attached to the membrane (20). In this model, membrane deformations expose increased amounts of actin to cystic fibrosis transmembrane conductance regulator (CFTR), a transmembrane protein that releases ATP on binding to actin.

Our results, however, show that stretching deformations alone are insufficient for the mechanotransduction of ATP. Rather, we propose that the two timescales observed in our experiments are associated with two distinct physical processes in the actin-CFTR model, which both must occur for ATP to be released. First, the 3- to 6-ms activation time is associated with the reorganization (i.e., relaxation) of the spectrin-actin network in response to the deformation. This process exposes additional actin to the cell membrane, where it can bind with CFTR. The second timescale is associated with the time required for CFTR to diffuse along the cell membrane and bind to the exposed actin. Given that the diffusion constant of CFTR is approximately $D = 10^{-13}$ m^2/s (31) and the interactin junction distance l_{act} ranges from 60 to 80 nm (32), on average it takes $t = l_{act}^2/D \approx$ 30–70 ms for CFTR to find actin. This timescale is comparable to our measured delay of 25–75 ms.

Moreover, our results show that the magnitude of ATP release is significantly decreased by the presence of diamide, but the average delay time is only weakly affected at most. Because diamide cross-links the spectrin network (29), a possible interpretation is that cross-linking reduces the amount of actin exposed to the membrane and thereby decreases the number of actin–CFTR complexes available to release ATP. The delay time remains unchanged at a given shear stress, however, because diamide only weakly affects the membrane viscosity (33) and the corresponding diffusivity of membrane-bound CFTR. In contrast, the membrane viscosity decreases with shear stress (34). Our observations of a decrease in delay time with increased shear stress might therefore be attributable simply to an increase in the diffusivity of CFTR at higher shear stress. Additional work is necessary to test this hypothesis.

In summary, we establish a microfluidic approach to study the dynamics of shear-induced ATP release from RBCs with millisecond resolution. We demonstrate that there are two distinct timescales for ATP release, an activation time and a mechanotransduction delay time. We hypothesize that these times are related to a two-step cellular mechanotransduction pathway, which is consistent with an actin–CFTR association model. However, other ion channels have been implicated in mechanosensitive ATP release from RBCs (22). The relative importance of each channel, and possible connections between different biochemical pathways, are unclear. The experimental procedure developed here will be useful to elucidate the dynamics of mechanotransductive behavior at the whole-cell level, not only for RBCs and ATP, but ultimately also for other types of mechanosensing cells and signaling molecules.

Materials and Methods

Microfluidic Fabrication. Standard soft photolithographic techniques were used to fabricate microchannels in polydimethylsiloxane (PDMS) (35). To begin an experiment, a suspension of cells was loaded in a syringe (Hamilton) and connected to a syringe pump (Kd Scientific, KDS101). Polyethylene (PE 20) tubes connected the syringe needle to the inlet hole in the device.

Luciferase Preparation. ATP sodium salt, D-luciferin, firefly luciferase, and diamide were purchased from Sigma. Physiological salt solution (PSS) was prepared by following the protocol in ref. 18: 4.7 mM KCl/2.0 mM $CaCl_2$/1.2 mM $MgSO_4$/140.5 mM NaCl/21.0 mM Tris(hydroxymethyl)aminomethane/11.1 mM dextrose with 1 mg/ml BSA, pH adjusted to 7.4. The luciferin/luciferase solution was prepared by adding 100 μl of 1 mg/ml luciferase and 1.5 mg of D-luciferin into 5 ml of PSS buffer. The ATP stock solution was prepared by adding 3 mg of ATP sodium salt in 10 ml of distilled, deionized water and then diluted with PSS buffer to specific concentrations. The luciferin/luciferase mixture and standard ATP solution were always prepared on the day of use.

RBC Preparation. The human RBCs used experimentally were extracted from individual healthy donors and prepared on the day of use. The RBCs were separated from plasma by centrifuging 3 ml of blood at 1,400 rpm at 20°C for 5 min. The supernatant and buffy coats were removed by aspiration. The packed RBCs were resuspended and washed three times in PBS buffer. The RBCs were then diluted with the PSS buffer to obtain a 10% RBC solution by volume. For high-speed visualization experiments, we dilute the hematocrit to 3% to make possible observations of individual cells in the constriction. Because the apparent viscosity of an RBC solution is approximately constant when the hematocrit is <10% (14), the shear stresses experienced by the RBCs are comparable to our previous experiments. For diamide-treated RBCs, 1 ml of 10% RBCs was incubated with 37 μM diamide for 20 min at room temperature and washed three times with PSS buffer before dilution with the luciferase/luciferin solution.

Light Measurement and High-Speed Video. The bioluminescent signal was measured at different positions along the channel by translating a 100× objective (N.A. = 0.75) on a microscope (Leica DMIRB). The light signal was amplified by a photomultiplier tube (Hamamatsu, model R1527P) installed in a housing with a high-voltage supply (Photon Technology International, model 814) and attached to the microscope through a C mount. By using a data acquisition program written in-house (Labview, National Instrument), the detected signal was recorded for 30 s for each data point. To prevent cell sedimentation, we gently shook and rotated the syringe before and after recording each data point and waited ≈30 s until the flow was steady before recording the next data point. Each experiment was repeated three to five times before changing the device or cell type. The background intensity, in the absence of luciferase, was 8 photons per second. All experiments were performed at room temperature (≈25°C) and the experiments with luciferase/luciferin were conducted in a darkroom with special precautions to eliminate all of the sources of ambient light.

An ATP calibration experiment was performed in a rectangular straight channel with 100 μm width. A series of luciferase/luciferin PSS buffer solutions with different ATP concentrations were injected into the channel at a flow rate of 3 μl/min and the resulting light signal was measured at a fixed position downstream from the channel entrance. The resulting calibration curve (Fig. S1) provided the approximate ATP concentration values (C_{ATP}) reported in Figs. 2 and 3.

High-speed video was acquired with a Phantom V7 camera (Vision Research) at 11,000 frames per second. The resulting movies were analyzed by using standard image analysis routines in Matlab (Mathworks).

ACKNOWLEDGMENTS. We thank the Harvard Nanoscale Science and Engineering Center for support of this research, E. H. Abraham, C. Best, G. Guidotti, and R. Horton for helpful discussions, and D. A. Donlan for assistance in procuring blood samples.

1. Ellsworth ML, Forrester T, Ellis CG, Dietrich HH (1995) The erythrocyte as a regulator of vascular tone. *Am J Physiol* 269:H2155–H2161.
2. Bergfeld GR, Forrester T (1992) Release of ATP from human erythrocytes in response to a brief period of hypoxia and hypercapnia. *Cardiovasc Res* 26:40–47.
3. Light DB, Capes TL, Gronau RT, Adler MR (1999) Extracellular ATP stimulates volume decrease in Necturus red blood cells. *Am J Physiol* 277:C480–C491.
4. Sprague RS, Ellsworth ML, Stephenson AH, Lonigro AJ (1996) ATP: The red blood cell link to NO and local control of the pulmonary circulation. *Am J Physiol* 271:H2717–H2722.
5. Schwiebert EM, Zsembery A (2003) Extracellular ATP as a signaling molecule for epithelial cells. *Biochim Biophys Acta* 1615:7–32.
6. Sprague RS, *et al.* (2003) Extracellular ATP signaling in the rabbit lung: Erythrocytes as determinants of vascular resistance. *Am J Physiol* 285:H693–H700.
7. Sprague RS, Ellsworth ML, Stephenson AH, Kleinhenz ME, Lonigro AJ (1998) Deformation-induced ATP release from red blood cells requires CFTR activity. *Am J Physiol* 275:H1726–H1732.
8. Sprague RS, Stephenson AH, Ellsworth ML, Keller C, Lonigro AJ (2001) Impaired release of ATP from red blood cells of humans with primary pulmonary hypertension. *Exp Biol Med* 226:434–439.
9. Sprague RS, Stephenson AH, Bowles EA, Stumpf MS, Lonigro AJ (2006) Reduced expression of Gi in erythrocytes of humans with type 2 diabetes is associated with impairment of both cAMP generation and ATP release. *Diabetes* 55:3588–3593.
10. Subasinghe W, Spence DM (2008) Simultaneous determination of cell aging and ATP release from erythrocytes and its implications in type 2 diabetes. *Anal Chim Acta* 618:227–233.
11. Abraham EH, *et al.* (1996) Cystic fibrosis hetero- and homozygosity is associated with inhibition of breast cancer growth. *Nat Med* 2:593–596.
12. Rapaport E, Fontaine J (1989) Anticancer activities of adenine nucleotides in mice are mediated through expansion of erythrocyte ATP pools. *Proc Natl Acad Sci USA* 86:1662–1666.
13. Bours MJL, Swennen ELR, Di Virgilio F, Cronstein BN, Dagnelie PC (2006) Adenosine 5′-triphosphate and adenosine as endogenous signaling molecules in immunity and inflammation. *Pharmacol Ther* 112:358–404.
14. Ganong WF (2003) in *Review of Medical Physiology*, eds Foltin J, Ransom MJ, Davis K (McGraw–Hill, New York), pp 587–590.
15. Fischer DJ, Torrence NJ, Sprung RJ, Spence DM (2003) Determination of erythrocyte deformability and its correlation to cellular ATP release using microbore tubing with diameters that approximate resistance vessels in vivo. *Analyst* 128:1163–1168.
16. Sprung R, Sprague R, Spence D (2002) Determination of ATP release from erythrocytes using microbore tubing as a model of resistance vessels in vivo. *Anal Chem* 74:2274–2278.
17. Moehlenbrock MJ, Price AK, Martin RS (2006) Use of microchip-based hydrodynamic focusing to measure the deformation-induced release of ATP from erythrocytes. *Analyst* 131:930–937.
18. Price AK, Fischer DJ, Martin RS, Spence DM (2004) Deformation-induced release of ATP from erythrocytes in a poly(dimethylsiloxane)-based microchip with channels that mimic resistance vessels. *Anal Chem* 76:4849–4855.
19. Price AK, Martin RS, Spence DM (2006) Monitoring erythrocytes in a microchip channel that narrows uniformly: Towards an improved microfluidic-based mimic of the microcirculation. *J Chromatogr* 1111:220–227.
20. Gov NS, Safran SA (2005) Red blood cell membrane fluctuations and shape controlled by ATP-induced cytoskeletal defects. *Biophys J* 88:1859–1874.
21. Hamill OP, Martinac B (2001) Molecular basis of mechanotransduction in living cells. *Physiol Rev* 81:685–740.
22. Locovei S, Bao L, Dahl G (2006) Pannexin 1 in erythrocytes: Function without a gap. *Proc Natl Acad Sci USA* 103:7655–7659.
23. Tangelder GJ, Slaaf DW, Arts T, Reneman RS (1988) Wall shear rate in arterioles in vivo: Least estimates from platelet velocity profiles. *Am J Physiol* 254:H1059–H1064.
24. DeLuca M, McElroy WD (1974) Kinetics of the firefly luciferase catalyzed reactions. *Biochemistry* 13:921–925.
25. DeLuca M (1976) Firefly luciferase. *Adv Enzymol Relat Area Mol Biol* 44:37–68.
26. Faivre M, Abkarian M, Bickraj K, Stone HA (2006) Geometrical focusing of cells in a microfluidic device: An approach to separate blood plasma. *Biorheology* 43:147–159.
27. Miseta A, *et al.* (1993) Relationship between cellular ATP, K+, Na+, and Mg2+ concentrations in mammalian and avian erythrocytes. *Biochim Biophys Acta* 1175:133–139.
28. Abraham EH, Salikhova AY, Hug EB (2003) Critical ATP parameters associated with blood and mammalian cells: Relevant measurement techniques. *Drug Dev Res* 59:152–160.
29. Fischer TM, Haest CWM, Stoehr M, Kamp D, Deuticke B (1978) Selective alteration of erythrocyte deformability by sulfhydryl reagents. Evidence for an involvement of spectrin in membrane shear elasticity. *Biochim Biophys Acta* 510:270–282.
30. Becker PS, Cohen CM, Lux SE (1986) The effect of mild diamide oxidation on the structure and function of human erythrocyte spectrin. *J Biol Chem* 261:4620–4628.
31. Haggie PM, Stanton BA, Verkman AS (2002) Diffusional mobility of the cystic fibrosis transmembrane conductance regulator mutant, DF508-CFTR, in the endoplasmic reticulum measured by photobleaching of GFP-CFTR chimeras. *J Biol Chem* 277:16419–16425.
32. Byers TJ, Branton D (1985) Visualization of the protein associations in the erythrocyte membrane skeleton. *Proc Natl Acad Sci USA* 82:6153–6157.
33. Engelhardt H, Sackmann E (1988) On the measurement of shear elastic moduli and viscosities of erythrocyte plasma membranes by transient deformation in high frequency electric fields. *Biophys J* 54:495–508.
34. Chien S, Sung K-LP, Skalak R, Usami S, Tozeren A (1978) Theoretical and experimental studies on viscoelastic properties of erythrocyte membrane. *Biophys J* 24:463–487.
35. Duffy DC, McDonald JC, Schueller OJA, Whitesides GM (1998) Rapid prototyping of microfluidic systems in poly(dimethylsiloxane). *Anal Chem* 70:4974–4984.